

Transport Gap in Suspended Bilayer Graphene at Zero Magnetic Field

A. Veligura,^{1,*} H.J. van Elferen,² N. Tombros,¹ J.C. Maan,² U. Zeitler,² and B.J. van Wees¹

¹*Physics of Nanodevices, Zernike Institute for Advanced Materials,
University of Groningen, Nijenborgh 4, 9747 AG Groningen, The Netherlands*

²*High Field Magnet Laboratory and Institute for Molecules and Materials,
Radboud University Nijmegen, Toernooiveld 7, 6525 ED Nijmegen, The Netherlands*

(Dated: March 29, 2012)

We report a change of three orders of magnitudes in the resistance of a suspended bilayer graphene flake which varies from a few k Ω s in the high carrier density regime to several M Ω s around the charge neutrality point (CNP). The corresponding transport gap is 8 meV at 0.3 K. The sequence of appearing quantum Hall plateaus at filling factor $\nu = 2$ followed by $\nu = 1$ suggests that the observed gap is caused by the symmetry breaking of the lowest Landau level. Investigation of the gap in a tilted magnetic field indicates that the resistance at the CNP shows a weak linear decrease for increasing total magnetic field. Those observations are in agreement with a spontaneous valley splitting at zero magnetic field followed by splitting of the spins originating from different valleys with increasing magnetic field. Both, the transport gap and B field response point toward spin polarized layer antiferromagnetic state as a ground state in the bilayer graphene sample. The observed non-trivial dependence of the gap value on the normal component of B suggests possible exchange mechanisms in the system.

PACS numbers: 73.22.Pr, 72.80.Vp, 73.43.Qt, 85.30.Tv

Keywords: suspended bilayer graphene, spontaneous gap, quantum Hall effect, magnetoresistance

I. INTRODUCTION

Followed by the isolation of single layer graphene, the study of bilayer graphene (BLG) became a separate direction of research in the community of two dimensional materials. Charge carriers in bilayer graphene have a parabolic dispersion with an effective mass of about $0.054m_e$,^{1,2} but also possess a chirality. The latter manifests itself in an unconventional quantum Hall effect³ with the lowest Landau level (LLL) being eight fold degenerate. Compared to single layer, bilayer graphene has next, to spin and valleys degrees of freedom, an additional orbital degree of freedom, where Landau levels with numbers $n = 0$ and 1 (each four fold degenerate) have the same energy.^{2,3} Recent advances in obtaining suspended bilayer graphene devices with charge carrier mobility exceeding $\mu > 10,000 \text{ cm}^2\text{V}^{-1}\text{s}^{-1}$ gave access to the investigation of many-body phenomena in clean bilayer graphene at low charge carrier concentration ($n < 10^{10} \text{ cm}^{-2}$).⁴⁻¹¹

Due to the non vanishing density of states at the charge neutrality point (CNP), bilayer graphene is predicted to have a variety of ground states triggered by electron-electron interaction. There are two competing theories describing the ground state of BLG: a transition (i) to a gapped layer polarized state (excitonic instability)¹²⁻¹⁷ or (ii) to a gapless nematic phase.¹⁸⁻²⁰

Excitonic instability is a layer polarization in which the charge density contribution from each valley and spin spontaneously shifts to one of the two graphene layers.^{16,17} This redistribution is caused by an arbitrarily weak interaction between charge from conduction and valence band states.^{12,13} Since each bilayer flavor (spin or valley) can polarize towards either of the two layers,

there are 16 possible states,^{16,17} which can be classified by the total polarization as being *layer* ferromagnetic (all degrees of freedom choose the same layer), *layer* ferromagnetic (three of the four valley-spin flavors choose the same layer), or *layer* antiferromagnetic (with no overall polarization). To make it clear, the term "*magnetic*" should be associated to flavors (not only spin) orientation in between two layers. These states are considered as analogous to the biased bilayer²¹ in the sense that the charge transfer can be attributed to the (wave vector dependent) exchange potential difference between low-energy sites on the opposite layers.¹⁶ The total energy of the system is lowered by the gain in the exchange interaction via breaking of the inversion symmetry, i.e. introducing a gapped state. Antiferromagnetic polarization is electrostatically favorable due to the absence of a net charge on both layers, however, the actual ground state is theoretically undefined.^{12,16,17} Recent experiments have suggested the evidence of the possible existence of two of the antiferromagnetic states - the anomalous quantum Hall state (AQH)^{5,6} and spin polarized layer antiferromagnetic state (LAF)⁷. To avoid possible confusion we note that in earlier literature¹⁶ the LAF state is also called quantum valley Hall state. The AQH has electrons being polarized in the same layer for both spins and in opposite layers for opposite valleys.^{16,17} This state has spontaneously broken time reversal symmetry and therefore possess a substantial orbital magnetization exhibiting quantized Hall effect (at zero magnetic field), while its spin density is everywhere zero.¹⁷ Due to its magnetization the AQH can be favored over other ground states in the perpendicular magnetic field. The LAF state has opposite spin-polarization for opposite layers. In contrast to AQH, the LAF state does not have topologically

protected edge states, which brings its minimum conductance to zero. For both states the theoretical estimations of the gap Δ give the value of 1.5-30 meV.^{13,16} However, the inter-valley exchange weakly favors the LAF state.^{16,22} One of the ways to determine the character of the bilayer ground state experimentally is to investigate the response of the gap value to the magnetic field B (which couples to spin) and electrical field E (which couples to layer pseudospin).²² When Zeeman coupling is included, the QAH state quasiparticles simply spin-split, leaving the ground state unchanged but the charge gap reduced. It was calculated that for a 4 meV spontaneous gap at zero-field, a field of $B = 35$ T drives the gap to zero. On the other hand, the gap of LAF is weakly B field dependent.

The second possible description for the ground state of BLG is based on a nematic phase caused by the renormalization of the low energy spectrum.^{18,19} Detailed tight-binding model studies showed that including next-neighbor interlayer coupling changes the band structure in bilayer producing a Lifshitz transition in which the isoenergetic line about each valley is broken into four pockets with linear dispersion.^{2,23} At the energies higher than 1 meV the four pockets merge into one pocket with the usual quadratic dispersion. Moreover, electron-electron interactions might result in the further energy spectrum transformation, where the number of low energy cones can be reduced to two near each of the two K points.^{18,19} In this case the minimum conductance of the bilayer graphene is supposed to be increased comparing to bilayer with parabolic dispersion ($8e^2/h$). This scenario was also supported by the experimental result on the suspended bilayer graphene in which strong spectrum reconstructions and electron topological transitions were observed.¹⁰

In this paper we present electric transport properties of suspended bilayer graphene by studying its behavior in tilted magnetic fields. At $B = 0$ T we observe the spontaneous opening of a gap by changing charge carrier density from the metallic regime ($n = 3.5 \times 10^{11} \text{ cm}^{-2}$) to the CNP. At a temperature of 1 K we measure a resistance increase from 5 k Ω up to 14 M Ω . The observation indicates the gapped ground state of the studied bilayer graphene with a value of 6.8 meV. Measurements in tilted magnetic field showed that the resistance at the CNP decreases with an increasing of magnetic field. Based on this we propose a possible scenario of the symmetry breaking in this bilayer graphene sample: Spontaneous valley splitting at zero magnetic field followed by the splitting of the spins originating from different valleys with increasing of B . Both, the gap value and its weak linear decrease with B , supports LAF as the ground state of the studied sample.

II. EXPERIMENTAL DETAILS

Suspended bilayer graphene devices were prepared using an acid free technique.^{24,25} We deposited highly ordered pyrolytic graphite on $n^{++}\text{Si}/\text{SiO}_2$ wafer (500 nm thick) which is covered with an organic resist LOR (1.15 μm). A standard lithography procedure is performed in order to contact bilayer graphene flakes (determined by their contrast in optical microscope) with 80 nm of Ti/Au contacts. A second electron beam lithography step is used to expose trenches over which graphene membrane becomes suspended. To achieve high quality devices we use current annealing technique by sending a DC current through the membrane (up to 1.1 mA) at the temperature of 4.2 K. While ramping up the DC current, simultaneously, we keep track of the sample resistance. Once the resistance reaches values in the order of 10 k Ω s we stop annealing and check the gate voltage dependence. We repeat this procedure till the appearance of a sharp resistance maximum at the CNP located close to zero V_g . More details on the current annealing procedure can be found in Tombros *et al.*²⁵ The studied device was 2 μm long and 2.3 μm wide. All measurements were performed in four-probe geometry (with contacts across the full width of graphene) at the temperatures from 4.2 K down to 300 mK. The four-probe method allows to eliminate contact resistances. As discussed below the resistance measurements consist of a superposition of longitudinal magnetoresistance (ρ_{xx}) and Hall-resistance (ρ_{xy}). The carrier density in graphene is varied by applying a DC voltage (V_g) between the back gate electrode ($n^{++}\text{Si}$) and the graphene flake. Based on serial capacitors model a unit capacitance of the system is 7.2 aF μm^{-2} , which relates gate voltage with density as $n = \alpha V_g$ where α is a leverage factor of $\alpha = 0.5 \times 10^{10} \text{ cm}^{-2} \text{ V}^{-1}$. The typical current we use is around 1 nA. See Appendix.

III. TEMPERATURE DEPENDENCE AND QUANTUM TRANSPORT

Our pristine samples are strongly p-doped with the CNP situated beyond 60 V and a metallic resistance of a few hundreds of Ω s over the entire voltage range. Therefore we perform current annealing technique in order to obtain high quality devices. In contrast to previous samples, in which each next step of current annealing tend to cause sharper change in the resistance values within the scanned region of V_g , the discussed bilayer sample already shows after the first current annealing step a high resistive region around the CNP (not shown). The next annealing step (1.1 mA) moves the charge neutrality point down to $V_g = 3$ V. However, surprisingly the resistance around CNP becomes 14 M Ω and reduces down to 5 k Ω in the metallic regime at $V_g = -60$ V (Fig. 1a, Inset). This fact points toward opening of a gap. The temperature dependence of the membrane from 4.2 K to 300 mK is shown in Fig. 1a. There is an essential change

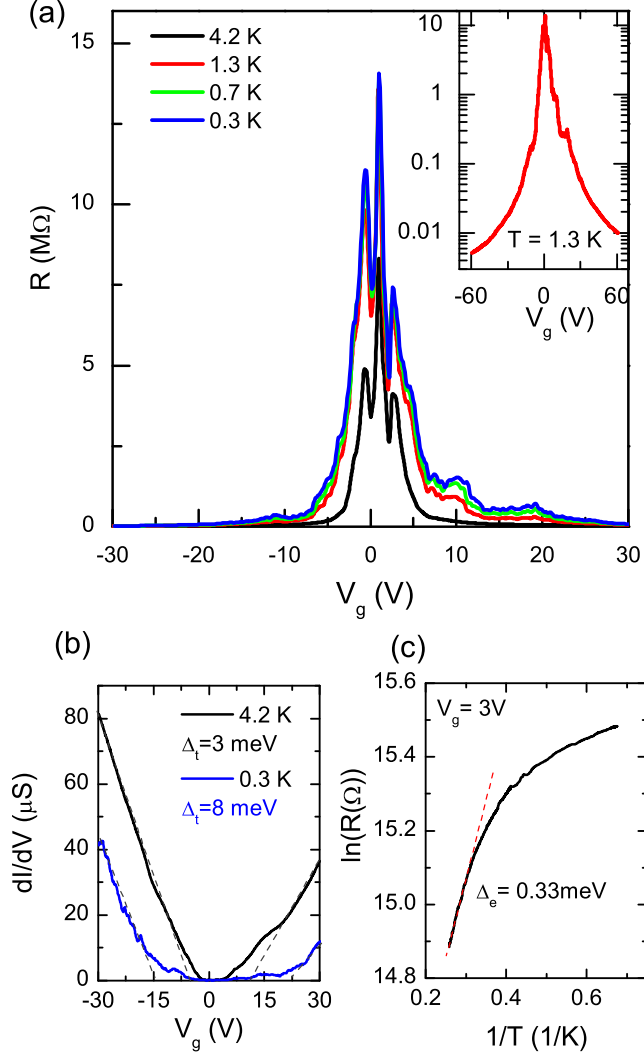


FIG. 1. (Color online) 4-Probe resistance of the suspended bilayer graphene. a) Gate dependence of the sample at the temperatures of 4.2 K (in black), 1.3 K (in red), 0.7 K (in green), 0.3 K (in blue). Inset: Resistance at 4.2 K in log-scale showing the dramatic change from the CNP to metallic regime; b) Transport gap extraction at 4.2 and 0.3 K. The energy gap in bias direction is highlighted by the conductance crossover (fitted with dashed lines) at zero. The values of the transport gap are 3 meV (4.2 K) and 8 meV (0.3 K); c) An Arrhenius plot of the resistance. The value of an extracted thermal gap is 0.33 meV

of about 6 MΩ in the maximum resistance (R_{max}) from 4.2 K down to 1.3 K, however further lowering of temperature does not change R_{max} much. From an Arrhenius plot of the resistance at CNP (Fig. 1c) we can extract a thermal excitation gap of 0.33 meV.²⁶ The saturation of resistance at lower T can be explained by a variable range hopping with different temperature dependence. We would like to point out that our excitation current value of 1 nA gave a voltage drop of $\propto 10$ mV at the CNP, which is much higher than kT energy at measured

temperatures (0.3 meV). Therefore one has to be careful in comparing transport and thermal excitation gaps.

There might be a couple of scenarios for the observed gap formation in the gate voltage dependence: (i) A lateral confinement in membrane, where energy levels are

$$E_n = \frac{\hbar^2 k^2}{2m} = \frac{\hbar^2 \pi^2}{2m W^2} l^2 \quad (1)$$

$W = 2.3 \mu\text{m}$ - width of the flake, l is integer value. However, first two levels have energies of $E_1 = 1.3 \mu\text{eV}$ and $E_2 = 5.3 \mu\text{eV}$, which is much lower than $k_B T$ at measured temperatures. (ii) True gap formation with zero density of states within the gap and available states at the conduction and valence bands. (iii) Transport gap, accompanied by the observation of the reproducible conductance oscillations in the region of suppressed conductance. In such regime transport is limited by the quantum confinement effect along the width (mainly originating from the impurities).²⁷ (iv) More complicated case, when the gap value depends on the charge carrier density, *i.e.* the energy of the levels changes while being filled with carriers. This situation might happen when the gap is induced by charge redistribution in between layers, which would be influenced by the applied back gate voltage. At the moment, we can not determine the exact gap type, therefore, further analysis is performed assuming a transport gap scenario, but keeping in mind that this gap value can depend on the density.

In an analogy to graphene nanoribbon studies^{27,28} we extract the transport gap from the gate dependence of the sample conductance as shown in Fig. 1b). From a linear approximation of conductance one gets a region of ΔV_g , where sample shows insulating behavior. This region ΔV_g relates to the wave vector as $\Delta k = \sqrt{\pi \Delta n} = \sqrt{\pi \alpha \Delta V_g}$. Taking into account the quadratic dispersion of bilayer graphene, the corresponding energy scale can be calculated as

$$\Delta E_F = \frac{\hbar^2 k^2}{2m} = \frac{\hbar^2}{2m} \pi \alpha \Delta V_g \quad (2)$$

From conductance graphs at different T we find $\Delta E_F = 3 \text{ meV}$ at 4.2 K and $\Delta E_F = 8 \text{ meV}$ at 0.3 K. The values of the transport gap are comparable to the energy gap (extracted in bias direction) values of single layer graphene nanoribbons of 50-85 nm wide,^{27,28} where in contrast to our case the gap is created by lateral confinement. The resistance value of 5 kΩ in metallic regime, similar to regular graphene devices, serves as an additional justification of excluding a lateral confinement as a cause of the observed transport gap. We can calculate the mobility of the charge carriers using a standard formula $\mu = 1/(e R_{sq} n)$, where R_{sq} is a square resistance of the sample and e is elementary charge. The mobility value $\mu \propto 20,000 \text{ cm}^2 \text{V}^{-1} \text{s}^{-1}$ at $n = 3.5 \times 10^{11} \text{ cm}^{-2}$ corresponds to the value of high quality bilayer graphene devices. Due to the symmetry of resistance change around CNP (Fig. 1b) and the fact that CNP itself is situated

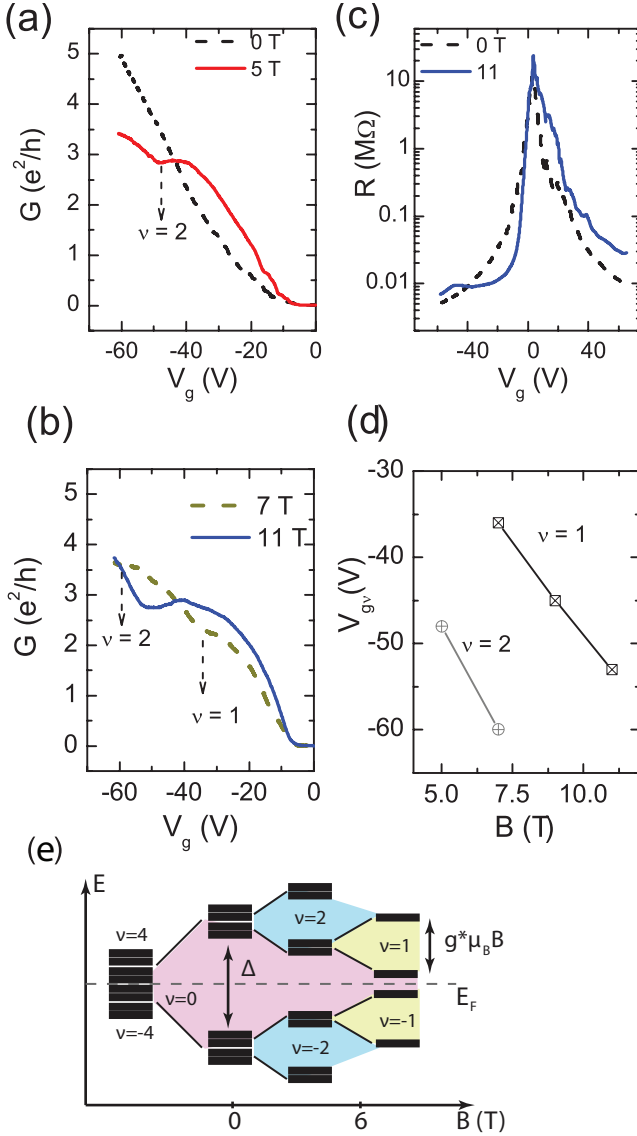


FIG. 2. (Color online) Quantum transport at 1.3 K. a) Quantum Hall conductance of the suspended bilayer at zero and $B = 5$ T; b) Quantum Hall conductance of the suspended bilayer at $B = 7$ and 11 T. The exact filling factors ν corresponding to the observed plateaus are shown; c) Resistance of the sample in quantum Hall regime. d) Scaling of the filling factors position in gate voltage ($V_{g\nu}$) with magnetic field; e) LL hierarchy of the symmetry-breaking of the lowest LL in bilayer graphene. Suggested scenario of the spontaneous valley splitting followed by the spin splitting at high B .

around zero gate voltage ($V_g = 1.2$ V), that corresponds to the density of $n = 0.77 \times 10^{10} \text{ cm}^{-2}$ at 0 V, we can also exclude the low quality "p-doped" regions close by the contacts (which can form after current annealing) as the cause of the reported gap. In the meantime, we can not exclude a charge inhomogeneity in the sample bulk which might lead to the observed order of magnitude difference between electrical and transport gaps, in analogy to nanoribbon case.

Given the fact that the resistance values reach MΩs at the CNP, it is already hard to establish quantum Hall plateaus in our suspended bilayer device. However, we have achieved to observe quantum Hall transport shown in Fig. 2a,b). First quantum Hall plateau appears at 5 T on electron side (red curve), which we attribute to the filling factor $\nu = 2$. This plateau is followed by the appearance of $\nu = 1$ at 7 T (Fig. 2b). The conductance values of the observed plateaus deviate from the expected ones of $2e^2/h$ and $1e^2/h$, since they are affected by charge inhomogeneity. Therefore, we determine the exact values of the corresponding plateaus by the scaling of their positions in density ($V_{g\nu}$) with magnetic field B (Fig. 2d). As expected from $\nu = n/(eB/h)$ the scaling is linear with the leverage factor of $\alpha = 0.64 \times 10^{10} \text{ cm}^{-2} \text{ V}^{-1}$ for $\nu = 2$ and 1 . In order to use the same α for both filling factor sets (see Fig. 2d) the slopes of $V_{g\nu}$ versus B ; and ν values respectively, have to be twice as different. Therefore, we have to point out that the linear scaling will hold as well for a leverage factor of $1.1 \times 10^{10} \text{ cm}^{-2} \text{ V}^{-1}$ in case we assume $\nu = 4$ and 2 as an observed sequence of plateaus. From previous studies²⁹ we know that capacitance probed by the QHE in graphene devices (especially in suspended samples) can be higher than the geometrical value, due to the deviation from the plane capacitor model. However, we attribute the observed plateaus to the filling factors 2 and 1 . As we noticed before,^{8,24} most of the time the current annealing procedure leads to the formation of high quality annealed regions connected in series with low mobility p-doped regions close to the contacts. Therefore higher values of the conductance plateaus can be explained by a "p-doped" slope, which increases with magnetic field B . This can be also the reason of the absence of resistance quantization in the electron-side (Fig. 2c). Assuming $\mu B \gg 1$ for the formation of QHE plateaus,³⁰ our observation implies a lower bound for the mobility of $2,000 \text{ cm}^2 \text{ V}^{-1} \text{ s}^{-1}$.

To summarize our QH transport results: At this point we have shown that a zero-field gap opens at the CNP in the studied graphene bilayer. This observation points out on a possible symmetry breaking of the ground state in bilayer graphene. The application of B does not restore the broken symmetry and brings the systems in to the QH regime. In Fig. 2e) we show the hierarchy of the splitting of the 8-fold degenerate lowest Landau level in applied B .³¹ The development of the level structure with B will be specified and discussed in section 4. In the meanwhile, if we assume that at $B = 0$ T one of the degeneracies is already lifted, then, with increasing field, one can expect quantization at the filling factors $\nu = 0$ and 4 followed by $\nu = 2$ and 1 . However, if the initial symmetry breaking is strong enough and the scanned window in energy is limited (V_g), then one can expect quantization at $\nu = 2$ followed by $\nu = 1$. This described hierarchy of levels splitting and sequence of plateaus will be observed independent on either valleys or spin splitting first.

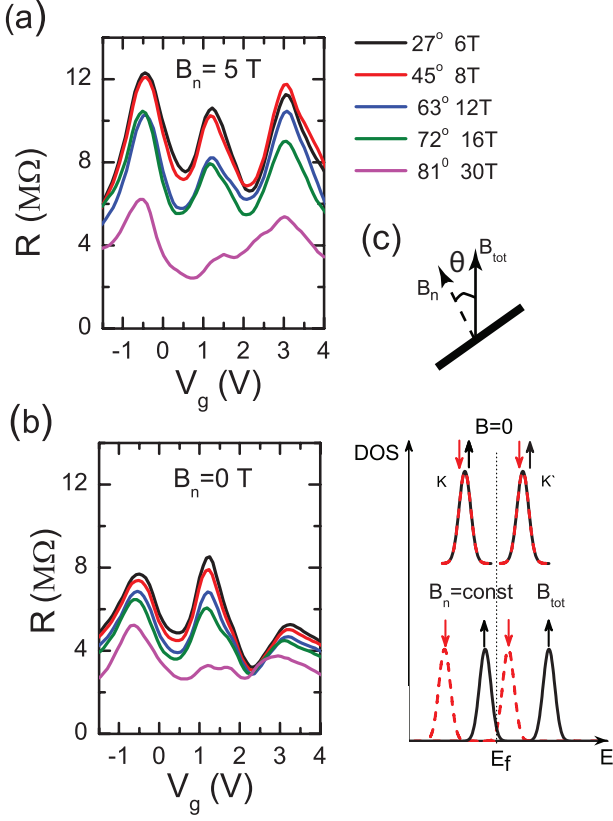


FIG. 3. (Color online) a) Behavior of the resistance at the charge neutrality point at fixed B_n and increasing B_{tot} . From top to bottom angle and total field: 27° (6 T), 45° (8 T), 63° (12 T), 27° (6 T), 72° (16 T), 81° (30 T) b) Behavior of the resistance at the charge neutrality point when B has only in plane field component ($\theta = 90^\circ$). c) Suggested scheme of the spontaneously split valley followed by spin splitting induced by B .

IV. RESISTANCE AT THE CNP IN TILTED MAGNETIC FIELD

In order to clarify the nature of the gapped ground state of bilayer graphene and its evolution in magnetic field we perform a tilted magnetic field experiment. In tilted experiments the total magnetic field (B_{tot}) can be separated from its normal (to the plane of the sample) component: $B_n = B_{tot} \cos \theta$, where θ is an angle between these two vectors (Fig. 3c). This procedure allows us to distinguish between the orbital effect (QHE) and pure Zeeman energy, which has to scale with B_{tot} value.^{22,31,32}

All measurements presented below were performed at a temperature of 1.3 K. The application of the magnetic field perpendicular to the sample plane leads to an increase in the resistance at the CNP, as it is expected for a QH transport in the case of broken symmetry states. To distinguish between normal component and total B we perform a series of experiments with keeping B_n fixed and gradually increasing B_{tot} . As an example, in Fig. 3a) we show a change in R_{max} at $B_n = 5$ T and B_{tot} increas-

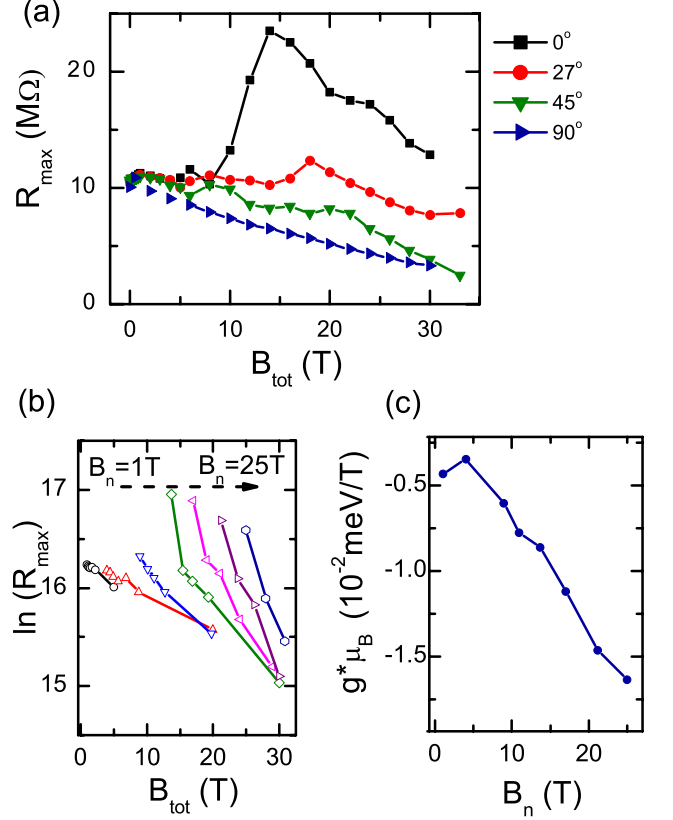


FIG. 4. (Color online) (a) Change in the R_{max} of the middle peak with total magnetic field B_{tot} . (b) $\ln(R_{max})$ as a function of B_{tot} at different B_n . The values of B_n from left to right 1, 4, 9, 13.7, 17, 21.2, 25 T. (c) The slope of the linear fit from Fig. 4b) as a function of normal component B_n .

ing from 6 T up to 30 T for different angles θ . The actual maximum of the resistance consists of three peaks: highly resistive in the middle ($V_g = 1.2$ V) and two side peaks at the gate voltage at -0.5 and 3 V. The total magnetic field causes decrease in the resistance and the middle peak starts splitting into two peaks (or developing minimum in resistance at the CNP) when $B_{tot} > 6$ T for studied values of B_n . We observe exactly the same behavior in the experiment when $B_n = 0$ and applied field is in parallel to the graphene membrane: maximum of the resistance goes down and develops a local minimum at the CNP (Fig. 3b). We attribute this change with an increase of the total magnetic field. That fact that resistance changes with B_{tot} indicates that observed effect is not a simple quantum localization due to inhomogeneity in the sample.

All three maxima around the CNP decrease in their resistance in applied parallel B . However, only the middle maximum at $V_g = 1.2$ V shows clear scaling with the total magnetic field (B_{tot}) at different tilted angles θ (Fig. 4a). As one can see in the case of $B_{tot} = B_n$ ($\theta = 0$, black curve in Fig. 4a) the resistance keeps on increasing up to around 14 T; further increase in magnetic field brings

R_{max} to lower values (Fig. 4a). Once the non zero angle is introduced the common trend for R_{max} is a decrease.

We suggest that the behavior of the middle peak is caused by the many-body effect and can be explained by the Zeeman splitting closing the spontaneous gap. The hierarchy of energy levels is depicted in Fig. 2e). Once B value is high enough the LLL is split in to 4 levels, each two-fold degenerate. If we assume that the latter degeneracy is spin, then after the appearance of plateau associated with filling factor $\nu = 1$ we expect the value of the ground state gap Δ to be lowered by spin splitting coupled to B_{tot} . Here we would like to emphasize, that we do observe appearance of $\nu = 1$ and minimum of resistance at the CNP in similar magnetic field $B_{tot} > 7$ T. In a simplified way we describe resistance value at the CNP point as

$$\ln R_{max} \propto \Delta/(kT) - g^* \mu_B B_{tot}/(kT), \quad (3)$$

where g^* is an effective g -factor including exchange electron interaction and a Landau level broadening.^{8,32,33} The change in $\ln(R)$ versus B_{tot} at fixed B_n values is shown in Fig. 4b). This dependence can be the best described as linear. The slope and y-intercept of the linear fit of Fig. 4b) give the values of Δ and $g^* \mu_B$. Surprisingly, these both contributions scale with B_n component. In Fig. 4c) we show $g^* \mu_B$ values versus B_n . Despite the fact that the scaling seems like linear, plotting the slope as a function of $\sqrt{B_n}$ does seem like fitting as well (not shown). Δ value increases with B_n from 1.4 meV at $B_n = 1$ T up to 1.7 meV at $B_n = 25$ T (not shown). This Δ is of the same order as the measured transport gap (which can overestimate a real energy gap) and also corresponds to the theoretically predicted gap of 1.5-30 meV for the excitonic instability.^{13,16,22}

In summary, tilted magnetic field experiments show that the resistance at the CNP of studied gapped bilayer graphene decreases linearly with the total magnetic field component. This points to a many-body effect and weak reduction of the gap in applied magnetic field. The developed minimum in the resistivity in Fig. 3 can be explained by the overlapping of spin-up and spin-down levels from the adjacent Landau levels due to Zeeman splitting in applied B .³³ However, from our experiments the estimated $g^* < 0.2$, which is very low for spin splitting. In addition, although the resistance decreases in parallel field, the R_{max} value does not change an order of magnitude. This behavior in B is consistent with the layer antiferromagnetic state as a ground state of studied bilayer sample.²² Since in this state the top and bottom layers host spins with opposite orientations, their interaction with applied B can not be described as a simple Zeeman splitting. Next to it, our results also open an additional question: What is the role of exchange energy and level broadening Γ in LAF state? Naively, scaling of $g^* \mu_B$ with B_n can be understood from their dependence on level broadening Γ . The Γ value scales with $\sqrt{B_n}$, meaning the bigger B_n the smaller B_{tot} is needed to observe level's overlapping. In reality the situation can

be much more complicated including possible exchange mechanisms we do not understand yet. This is also supported by the fact that the ground state gap Δ depends on B_n as well.

Based on these results we suggest a possible scenario of symmetry breaking in high quality bilayer graphene (Fig. 2e and Fig. 3c). First splitting is caused by valleys, which results in the observed transport gap. An application of magnetic field induces spin splitting of both K and K' levels. When B is high enough then the energy of spin-up level from K will start approaching the spin-down level from K' . The overlapping of the levels will cause a decrease in the resistance at the charge neutrality point. Since we do observe transport gap in our sample, we exclude nematic phase transition. In addition to this, the response of the sample in tilted B fits to the LAF state. The cause of the valley splitting can be a combination of two effects: electron-electron interaction (which determines the B field behavior of the middle resistance maximum) and a contamination of the sample surface with charged impurities which break inversion symmetry (via introduction of electrical field).²¹

V. CONCLUSIONS

We report a transport gap of 3 meV in suspended bilayer graphene at 4.2 K, which increases with decreasing of temperature. The sequence of appearance of the QHE plateaus at the filling factor $\nu = 2$ followed by $\nu = 1$ supports a suggestion that the observed gap caused by the symmetry breaking. Measurements in the tilted magnetic field indicates that the resistance at the CNP shows weak linear decrease with the total magnetic field component. Based on this we propose a possible scenario of the symmetry breaking in the investigated bilayer graphene: Spontaneous valley splitting at zero magnetic field followed by the splitting of the spins originating from different valleys with increasing of B . The gap value and weak response of the sample to applied magnetic field corresponds to the predicted spin polarized layer antiferromagnetic state as a ground state of the investigated sample. The observed non-trivial dependence of the gap value from the normal component of B suggests possible exchange mechanisms in the system.

ACKNOWLEDGMENTS

We would like to thank B. Wolfs, M. de Roos and J.G. Holstein for technical assistance. We also thank M.H.D. Guimarães for useful discussions; and I.J. Vera-Marun for creating a soft-wear program for current annealing. This work is supported by NWO (via TopTalent grant), FOM, NanoNed and the Zernike Institute for Advanced Materials.

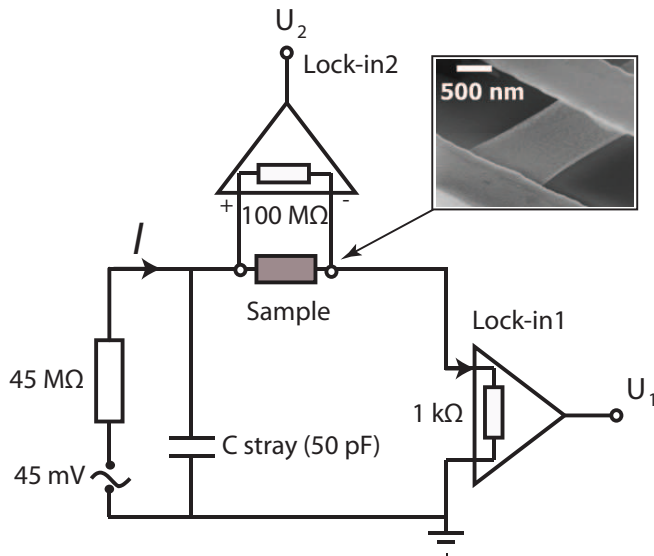


FIG. 5. (Color online) Electrical scheme of the setup we use to perform our measurements. Inset: Scanning electron micrograph of a typical suspended bilayer membrane in between two contacts.

VI. APPENDIX

In order to minimize self-heating in graphene at the high resistive CNP we used the following scheme (Fig. 5). An AC source maintained a fixed voltage amplitude of 45 mV (1.87 Hz frequency) across the sample in series with 45 MΩ resistor. The current through the sample is monitored by the lock-in1, whose output U_1 is proportional to the current flowing in the circuit ($U_1 = I \times 1\text{k}\Omega$). Simultaneously, the four probe voltage across the sample (U_2) is phase detected by another lock-in2 connected through the preamplifier having an input resistance up to 100 MΩ. Then the resistance of the sample is determined by $R = 1\text{k}\Omega \times U_2/U_1$. The power dissipating in the sample is $P = U_2^2/R$. Therefore, assuming that maximum V_2 is already reached ($\propto 10$ mV), with increasing of R the dissipation in the sample will be decreasing.

-
- * a.veligura@rug.nl
- ¹ E. McCann, Phys. Rev. B **74**, 161403 (2006).
 - ² E. McCann and V. I. Fal'ko, Phys. Rev. Lett. **96**, 086805 (2006).
 - ³ K. S. Novoselov, E. McCann, S. V. Morozov, V. I. Fal'ko, M. I. Katsnelson, U. Zeitler, D. Jiang, F. Schedin, and A. K. Geim, Nature Phys. **2**, 177 (2006).
 - ⁴ B. E. Feldman, J. Martin, and A. Yacoby, Nature Phys. **5**, 889 (2009).
 - ⁵ R. T. Weitz, M. T. Allen, B. E. Feldman, J. Martin, and A. Yacoby, Science **330**, 812 (2010).
 - ⁶ J. Martin, B. E. Feldman, R. T. Weitz, M. T. Allen, and A. Yacoby, Phys. Rev. Lett. **105**, 256806.
 - ⁷ J. J. Velasco, L. Jing, W. Bao, Y. Lee, P. Kratz, V. Aji, M. Bockrath, C. Lau, C. Varma, R. Stillwell, D. Smirnov, F. Zhang, J. Jung, and A. MacDonald, Nature Nano. **7**, 156 (2012).
 - ⁸ H. J. van Elferen, A. Veligura, E. V. Kurganova, U. Zeitler, J. C. Maan, N. Tombros, I. J. Vera-Marun, and B. J. van Wees, Phys. Rev. B **85**, 115408 (2012).
 - ⁹ F. Freitag, J. Trbovic, M. Weiss, and C. Schönenberger, Phys. Rev. Lett. **108**, 076602 (2012).
 - ¹⁰ A. S. Mayorov, D. C. Elias, M. Mucha-Kruczynski, R. V. Gorbachev, T. Tudorovskiy, A. Zhukov, S. V. Morozov, M. I. Katsnelson, V. I. Fal'ko, A. K. Geim, and K. S. Novoselov, Science **33**, 860 (2011).
 - ¹¹ W. Bao, J. Velasco, F. Zhang, L. Jing, B. Standley, D. Smirnov, M. Bockrath, A. MacDonald, and C. N. Lau, preprint, arXiv:1202.3212v1 (2012).
 - ¹² R. Nandkishore and L. Levitov, Phys. Rev. Lett. **104**, 156803 (2010).
 - ¹³ R. Nandkishore and L. Levitov, Phys. Rev. B **82**, 115431 (2010).
 - ¹⁴ H. Min, G. Borghi, M. Polini, and A. H. MacDonald, Phys. Rev. B **77**, 041407 (2008).
 - ¹⁵ F. Zhang, H. Min, M. Polini, and A. H. MacDonald, Phys. Rev. B **81**, 041402 (2010).
 - ¹⁶ J. Jung, F. Zhang, and A. H. MacDonald, Phys. Rev. B **83**, 115408 (2011).
 - ¹⁷ F. Zhang, J. Jung, G. A. Fiete, Q. Niu, and A. H. MacDonald, Phys. Rev. Lett. **106**, 156801 (2011).
 - ¹⁸ O. Vafek and K. Yang, Phys. Rev. B **81**, 041401 (2010).
 - ¹⁹ Y. Lemonik, I. L. Aleiner, C. Toke, and V. I. Fal'ko, Phys. Rev. B **82**, 201408 (2010).
 - ²⁰ C. Töke and V. I. Fal'ko, arXiv:0903.2435v1.
 - ²¹ E. V. Castro, K. S. Novoselov, S. V. Morozov, N. M. R. Peres, J. M. B. L. dos Santos, J. Nilsson, F. Guinea, A. K. Geim, and A. H. Castro Neto, Phys. Rev. Lett. **99**, 216802 (2007).
 - ²² F. Zhang and A. H. MacDonald, arXiv:1107.4727v1.
 - ²³ E. McCann, D. S. Abergel, and V. I. Fal'ko, Solid State Commun. **143**, 110 (2007).
 - ²⁴ N. Tombros, A. Veligura, J. Junesch, J. J. van den Berg, P. J. Zomer, M. Wojtaszek, I. J. Vera-Marun, H. T. Jonkman, and B. J. van Wees, Jour. Appl. Phys. **109**, 093702 (2011).
 - ²⁵ N. Tombros, A. Veligura, J. Junesch, M. H. D. Guimaraes, I. J. Vera-Marun, H. T. Jonkman, and B. J. van Wees, Nature Phys. **7**, 697 (2011).
 - ²⁶ F. Xia, D. B. Farmer, Y.-m. Lin, and P. Avouris, NanoLetters **10**, 715 (2010).
 - ²⁷ F. Molitor, C. Stampfer, J. Güttinger, A. Jacobsen, T. Ihn, and K. Ensslin, Semicond. Sci. Technol. **25**, 034002 (2010).
 - ²⁸ C. Stampfer, J. Güttinger, S. Hellmüller, F. Molitor, K. Ensslin, and T. Ihn, Phys. Rev. Lett. **102**, 056403 (2009).

- ²⁹ I. J. Vera-Marun, P. Zomer, A. Veligura, M. H. D. Guimaraes, L. Visser, N. Tombros, H. J. van Elferen, U. Zeitler, and B. J. van Wees, arXiv:1112.5462v1.
- ³⁰ K. I. Bolotin, K. J. Sikes, Z. Jiang, M. Klima, G. Fudenberg, J. Hone, P. Kim, and H. L. Stormer, *Solid State Commun.* **146**, 351 (2008).
- ³¹ Y. Zhao, P. Cadden-Zimansky, Z. Jiang, and P. Kim, *Phys. Rev. Lett.* **104**, 066801 (2010).
- ³² E. V. Kurganova, H. J. van Elferen, A. McCollam, L. A. Ponomarenko, K. S. Novoselov, A. Veligura, B. J. van Wees, J. C. Maan, and U. Zeitler, *Phys. Rev. B* **84**, 121407 (2011).
- ³³ R. J. Nicholas, R. J. Haug, K. v. Klitzing, and G. Weimann, *Phys. Rev. B* **37**, 1294 (1988).